Refractive index sensing based on semiconductor nanowire lasers

Xiaoqin Wu,[1,2] Qiushu Chen,[1] Peizhen Xu,[2] Limin Tong,[2] and Xudong Fan[1,a)]
[1]*Department of Biomedical Engineering, University of Michigan, 1101 Beal Avenue, Ann Arbor, Michigan 48109, USA*
[2]*State Key Laboratory of Modern Optical Instrumentation, Department of Optical Engineering, Zhejiang University, Hangzhou 310027, People's Republic of China*

(Received 11 May 2017; accepted 11 July 2017; published online 20 July 2017)

We demonstrate a refractive index (RI) sensor based on semiconductor nanowire lasers. It is shown that the TE_{01} mode is responsible for lasing and sensing with the lasing threshold of 3 $\mu J/mm^2$ and the lasing peak width as narrow as 0.22 nm. A RI sensitivity of 21.2 nm/RIU (refractive index units), a figure of merit of approximately 100, and an RI detection limit of 1.4×10^{-3} RIU are achieved. *Published by AIP Publishing.* [http://dx.doi.org/10.1063/1.4995456]

Owing to their excellent optical and electrical properties, one-dimensional semiconductor nanowires (NWs) have shown great potential in developing nanoscale lasers, photodetectors, and photonic circuits,[1–5] as well as nanosensors for the detection of a wide range of chemicals and biological species.[6–17] To date, most of the NW sensors are in the form of field-effect transistors by taking advantage of the NWs' semiconducting properties, in which their conductance can be sensitively modulated by the binding of a charged analyte of interest.[6–15] On the other hand, due to their sub-micron diameter, NWs have an appreciable fraction of the electrical field outside their surface. In addition, the high refractive index (RI, $n > 2$) of the NWs allows the light to be reflected at the end-facet with high reflectivity and guided along the NW, thus forming a good Fabry-Perot (FP) cavity even when the NWs are immersed in liquid. The strong evanescent interaction with the surrounding environment and superior waveguiding capability can potentially be exploited for efficient excitation and collection of fluorescence from various nano-emitters (e.g., quantum dots and dyes), and for sensitive detection of the RI change near the NW surface. However, the NW sensors based on the aforementioned optical properties are rarely investigated. Evanescent or near-field fluorescence excitation and collection using NWs was demonstrated several years ago.[16,18] Only until recently was RI sensing reported by using the leaky resonant scattering of CdSe NWs with a diameter of 45–252 nm.[17] A maximal sensitivity 235 nm/RIU (refractive index units) was achieved. However, due to the extremely broad scattering peak (~100 nm), the figure-of-merit (FOM), defined as the ratio between the sensitivity and the peak width, is only 4.6 at the best, which considerably limits the NW's performance in RI sensing.

In this letter, we developed an RI sensor based on an optically pumped CdS NW laser, in which the lasing wavelength shifts in response to the RI change in the surrounding solution. In contrast to the broad peak of resonant scattering and photoluminescence spectrum of NWs, the NW laser has a peak width of 0.22 nm, resulting in a significantly improved FOM of approximately 100.

The laser based RI sensor investigated in this work is schematically illustrated in Fig. 1. The CdS ($n = 2.67$) NWs (240 nm in diameter and 16.6 μm in length) were grown on Si wafers using a chemical vapor transport process.[19] As-synthesized NWs were directly deposited on a silica cover glass, which was then exposed to low-pressure plasma with continuous air flow for about 1 min. Such plasma treatment promoted the immobilization of the NWs on the glass surface,[20] which is essential to experiments in the liquid environment. Finally, a polydimethylsiloxane (PDMS) fluidic channel was bonded to the cover glass for liquid sample delivery.

To investigate the lasing characteristics of the NW in liquid, the CdS NW was excited by a pulsed optical parametric oscillator (5 ns pulse width, 20 Hz repetition rate, wavelength = 479 nm). The pump beam was focused with a 50 × objective lens with a focal spot size of 60 μm. The emitted light scattered from the NW end-facets was collected by the same objective lens and directed to a spectrometer with a resolution of 0.02 nm (Horiba iHR550 with a 2400 g mm^{-1} grating). Figure 2(a) shows typical lasing spectra of the NW immersed in ethanol ($n = 1.365$) under different pump energy densities, with a dominant lasing peak centered around 504.3 nm and the corresponding linewidth of 0.22 nm. The free spectral range (FSR) is measured to be 1.67 nm. A lasing threshold of about 3 $\mu J/mm^2$ can be deduced from Fig. 2(b)

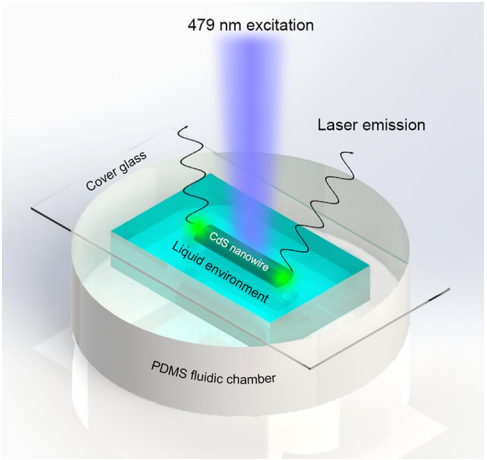

FIG. 1. Schematic of the RI sensor based on a CdS NW laser. The NW was immobilized on the lower surface of a cover glass and surrounded by the solution to be detected. A PDMS channel was added for sample delivery.

a)Author to whom correspondence should be addressed: xsfan@umich.edu

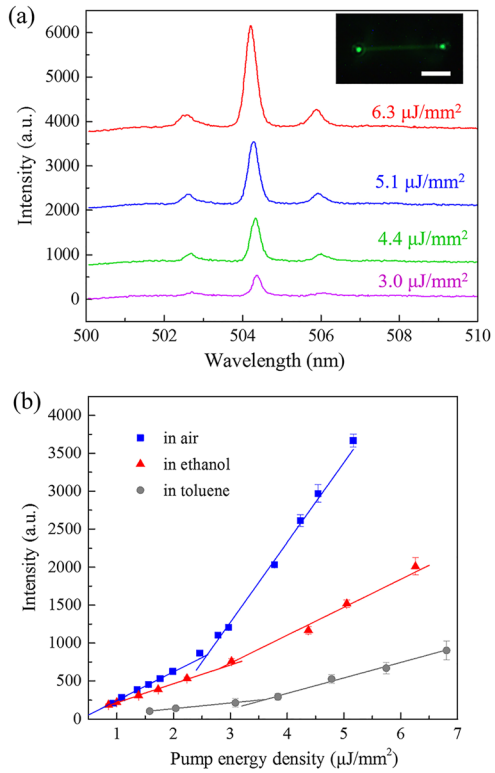

FIG. 2. (a) Lasing spectra collected from the left end-facet of the CdS NW in ethanol under various pump energy densities. Curves are vertically shifted for clarity. Inset: CCD image of the lasing CdS NW at a pump energy density of 6.3 μJ/mm^2. Scale bar, 5 μm. (b) Spectrally integrated (500 nm–508 nm) laser output as a function of pump energy density for the CdS NW immersed in air (n = 1), ethanol (n = 1.365), and toluene (n = 1.505), respectively. Error bars were obtained with 5 measurements.

(red triangles). Compared to the same NW in air (blue squares), the threshold for the NW in ethanol is evidently increased with the reduced slope (or lasing efficiency), which may be attributed to the decreased reflectivity at the NW end-facets in the presence of surrounding medium of a higher RI. The same trend can also be observed when the NW was immersed in toluene that has even higher RI (n = 1.505).

For RI sensing, we immersed the NW in the mixed solution of ethanol and toluene with volume ratios of 10:0, 9:1, 8:2, and 7:3, which correspond to RIs of 1.365, 1.379, 1.393, and 1.407, respectively. Figure 3(a) shows lasing spectra obtained for each RI under the same excitation energy density of 4 μJ/mm^2. In most cases, the NW operates in multi-mode, with one dominant peak and two side modes. We used the dominant peak wavelength in ethanol [denoted by the arrow in the red curve in Fig. 3(a)] as the RI indicator and monitored its evolution as the RI changes. A significant red shift from 504.35 nm to 505.23 nm can be observed when the RI increases from 1.365 to 1.407. Accompanied with this process is the graduate degradation of the dominant peak into a side lasing mode. The dependence of the NW laser on the RI change is plotted in Fig. 3(b), showing a sensitivity of 21.2 nm/RIU. Given the linewidth of the lasing peak of 0.22 nm, an FOM of 96 is obtained, which represents 24-fold improvement over the recent result using the resonant scattering.[17] Compared to the lasing enhanced surface plasmon resonance sensors,[21,22] while they have a similar FOM and lasing threshold, the semiconductor NW sensor is less complicated

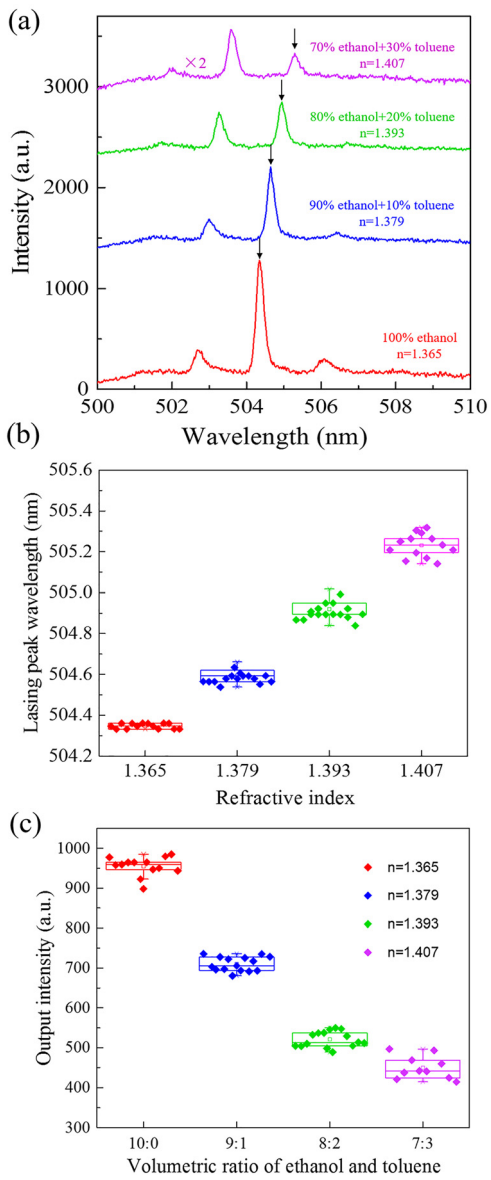

FIG. 3. (a) Lasing spectra of the NW laser sensor in the mixed solution of ethanol and toluene with different volume ratios of 10:0 (red line), 9:1 (blue line), 8:2 (green line), and 7:3 (purple line) under the same pump energy density of 4 μJ/mm^2. The arrow indicates the same resonant mode of the lasing NW. (b) Lasing peak wavelength of the NW versus RI of surrounding medium. The value of peak wavelength is extracted from the same lasing mode indicated by the arrow in (a). The lasing spectra were measured 15 times for each RI. (c) Spectrally integrated (500 nm–508 nm) laser output of the NW in different RIs.

to fabricate and can be readily internalized into the cells.[23,24] The long-term stability of the lasing wavelength was investigated over 30 min, showing a standard deviation of about 0.03 nm for RI = 1.365 (red squares) under study, which results in an RI detection limit down to 1.4×10^{-3} RIU. As the surrounding RI increases to 1.407 (purple squares), the variation in the resonance wavelength becomes larger (standard deviation: ~0.1 nm), which is due to the fact that the lasing mode that we monitor gradually shifts out of the peak of the gain profile and thus becomes weaker and broader.

In the experiment, we noticed that the entire lasing output intensity (integrated from 500 to 508 nm) at the constant pump energy density could also be used for RI detection (note that the absorption of toluene and ethanol at the

wavelength range of 500–510 nm can be neglected[25]). One of the advantages of this RI sensing scheme is that no high-resolution spectrometer is needed. As shown in Fig. 3(c), when RI increases from 1.365 to 1.407, the output intensity decreases, which is caused by the decreased Q-factor of the FP cavity (and hence the increased lasing threshold) that results from the reduced NW end-facet reflectivity [see also Fig. 2(b)]. The corresponding RI sensitivity is estimated to be 1.2×10^4 counts/RIU with the detection limit 4×10^{-3} RIU.

It is well known that the transverse mode in the lasing NW is critical to determining the RI sensitivity of the laser. However, the CdS NW with a 240-nm diameter can support multiple transverse modes: HE_{11}, TE_{01}, TM_{01}, and HE_{21} mode. To better understand which mode is responsible for sensing, we calculate the sensitivity for all these modes using finite-difference time-domain (FDTD). Specifically, for the NW with a fixed diameter (D = 240 nm) and a specific surrounding medium RI, the effective refractive index, $n_{eff}(\lambda)$, can be readily obtained in FDTD for a wide wavelength range. The dielectric constant of CdS at wavelength of 500 nm–510 nm is obtained from Ref. 26. Since the longitudinal mode order $m = 2n_{eff}(\lambda)L/\lambda$ should be an integer, where L is the cavity length, which is equivalent to the NW length, the resonance wavelength of each transverse mode (HE_{11}, TE_{01}, TM_{01}, and HE_{21} mode) can be derived. Here we take $HE_{11}^{(151)}$ (m = 151), $TE_{01}^{(123)}$ (m = 123), $TM_{01}^{(107)}$ (m = 107), and $HE_{21}^{(103)}$ (m = 103) mode and plot their respective RI-dependent wavelength in Fig. 4. The sensitivity of the HE_{11}, TE_{01}, TM_{01}, and HE_{21} mode is 12.8 nm/RIU, 19.8 nm/RIU, 86.9 nm/RIU, and 64.9 nm/RIU, respectively. Compared to our experimental sensitivity of 21.2 nm/RIU, the calculated value of the TE_{01} mode shows the best match.

For further verification, the FSR for the aforementioned modes of the NW in ethanol at wavelength around 504.4 nm is also investigated, which can be written as

$$FSR = \lambda^2/\left[2L(n_{eff} - \lambda dn_{eff}/d\lambda)\right]. \quad (1)$$

For the HE_{11}, TE_{01}, TM_{01}, and HE_{21} mode, the waveguide group index $n_g = n_{eff} - \lambda dn_{eff}/d\lambda$ is 4.249, 4.47, 4.03, and 4.87, corresponding to an FSR of 1.8 nm, 1.71 nm, 1.9 nm, and 1.57 nm, respectively. The calculated FSR value of the TE_{01} mode (1.71 nm) shows the best agreement with the experimental result (1.67 nm).

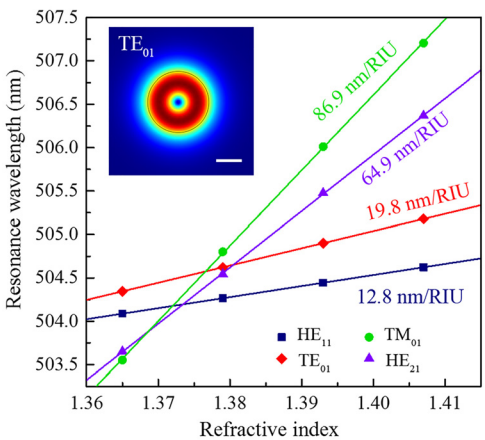

FIG. 4. Calculated resonance wavelength of the HE_{11}, TE_{01}, TM_{01}, and HE_{21} mode versus surrounding RI. Inset: electric field of TE_{01} mode of a 240-nm-diameter NW in ethanol at 504.3 nm wavelength, with 4.4% electric field energy outside the NW. Scale bar, 100 nm.

TABLE I. Lasing threshold for different transverse modes when surrounding RI is 1.365.

	HE_{11}	TE_{01}	TM_{01}	HE_{21}
R	11.8%	29.1%	5.5%	7.1%
Γ	1.07	1.1	0.75	1.05
g_{th} (cm^{-1})	1203	676	2330	1517

As a third evidence that the TE_{01} mode is responsible for lasing and RI sensing in this work, we calculate the lasing threshold for each mode, which is given by

$$\Gamma g_{th} = In(R^{-1})/L, \quad (2)$$

where Γ is the confinement factor, g_{th} is the material gain at the lasing threshold, and R is the reflectivity of the NW end-facet.[27–29] The calculated values of R, Γ, and g_{th} for different modes of NW in ethanol (RI = 1.365) are provided in Table I, which shows clearly that the gain needed to achieve lasing for the TE_{01} mode is far less than those for other modes, suggesting that the TE_{01} is the most likely lasing mode in the NW.[29]

In summary, we have demonstrated an RI sensor based on the CdS NW laser. Combined experimental results with theoretical analysis, we confirmed that it is the TE_{01} mode that is responsible for lasing and sensing, which helps better understand lasing NW sensors. Benefitting from the considerable fraction evanescent field of high-order mode (TE_{01}) and the narrow lasing peak width, the sensor based on detection of lasing wavelength shift shows a sensitivity of 21.2 nm/RIU and an FOM of 96. In addition, we showed that the lasing intensity variation at a fixed pump intensity can also be used for RI sensing due to the dependence of the lasing threshold on the surrounding RI. Our work suggests that the semiconductor NW laser is a promising technology for liquid sensing with a high sensitivity and FOM. In particular, due to its sub-micron diameter, the NW laser is uniquely positioned for intra-cellular sensing.

This work was supported by the National Science Foundation (ECCS-1607250) and the International Postdoctoral Exchange Fellowship Program (Grant No. 20160007). The authors wish to thank Yipei Wang for useful discussions and help in simulation.

[1]C. M. Lieber and Z. L. Wang, MRS Bull. **32**, 99 (2007).
[2]P. D. Yang, R. X. Yan, and M. Fardy, Nano Lett. **10**, 1529 (2010).
[3]C. M. Lieber, MRS Bull. **36**, 1052 (2011).
[4]Y. G. Ma, X. Guo, X. Q. Wu, L. Dai, and L. M. Tong, Adv. Opt. Photonics **5**, 216 (2013).
[5]S. W. Eaton, A. Fu, A. B. Wong, C. Z. Ning, and P. D. Yang, Nat. Rev. Mater. **1**, 16028 (2016).
[6]Y. Cui, Q. Q. Wei, H. K. Park, and C. M. Lieber, Science **293**, 1289 (2001).
[7]F. Patolsky and C. M. Lieber, Mater. Today **8**, 20 (2005).
[8]G. F. Zheng, F. Patolsky, Y. Cui, W. U. Wang, and C. M. Lieber, Nat. Biotechnol. **23**, 1294 (2005).
[9]P. H. Yeh, Z. Li, and Z. L. Wang, Adv. Mater. **21**, 4975 (2009).
[10]B. Z. Tian, T. Cohen-Karni, Q. Qing, X. J. Duan, P. Xie, and C. M. Lieber, Science **329**, 830 (2010).
[11]N. S. Ramgir, Y. Yang, and M. Zacharias, Small **6**, 1705 (2010).
[12]P. Feng, F. Shao, Y. Shi, and Q. Wan, Sensors **14**, 17406 (2014).

[13]N. Tiwale, Mater. Sci. Technol. **31**, 1681 (2015).
[14]A. Q. Zhang and C. M. Lieber, Chem. Rev. **116**, 215 (2016).
[15]J. F. Fennell, S. F. Liu, J. M. Azzarelli, J. G. Weis, S. Rochat, K. A. Mirica, J. B. Ravnsbaek, and T. M. Swager, Angew. Chem. Int. Ed. **55**, 1266 (2016).
[16]D. J. Sirbuly, M. Law, P. Pauzauskie, H. Yan, A. V. Maslov, K. Knutsen, C. Z. Ning, R. J. Saykally, and P. D. Yang, Proc. Natl. Acad. Sci. **102**, 7800 (2005).
[17]Y. L. Wang, B. W. Gao, K. Zhang, K. Yuan, Y. Wan, Z. Xie, X. L. Xu, H. Zhang, Q. J. Song, L. Yao, X. Fang, Y. P. Li, W. J. Xu, J. S. Zhang, and L. Dai, ACS Photonics **4**, 688 (2017).
[18]R. Yan, J. H. Park, Y. Choi, C. J. Heo, S. M. Yang, L. P. Lee, and P. D. Yang, Nat. Nanotechnol. **7**, 191 (2011).
[19]C. Ma and Z. L. Wang, Adv. Mater. **17**, 2635 (2005).
[20]M. D. Wiemer, J. Braeuer, D. Wünsch, and T. Gessner, ECS Trans. **33**, 307 (2010).
[21]X. Y. Wang, Y. L. Wang, S. Wang, B. Li, X. W. Zhang, L. Dai, and R. M. Ma, Nanophotonics **6**, 472 (2017).
[22]A. Yang, T. B. Hoang, M. Dridi, C. Deeb, M. H. Mikkelsen, G. C. Schatz, and T. W. Odom, Nat. Commun. **6**, 6939 (2015).
[23]J. H. Lee, A. Zhang, S. S. You, and C. M. Lieber, Nano Lett. **16**, 1509 (2016).
[24]J. F. Zimmerman, R. Parameswaran, G. Murray, Y. C. Wang, M. Burke, and B. Z. Tian, Sci. Adv. **2**, e1601039 (2016).
[25]S. Kedenburg, M. Vieweg, T. Gissibl, and H. Giessen, Opt. Mater. Express **2**, 1588 (2012).
[26]T. M. Bieniewski and S. J. Czyzak, J. Opt. Soc. Am. **53**, 496 (1963).
[27]A. V. Maslov and C. Z. Ning, Appl. Phys. Lett. **83**, 1237 (2003).
[28]A. V. Maslov and C. Z. Ning, IEEE J. Quantum Electron. **40**, 1389 (2004).
[29]M. A. Zimmler, F. Capasso, S. Müller, and C. Ronning, Semicond. Sci. Technol. **25**, 024001 (2010).